Journal of Power Sources 265 (2014) 45–49

Contents lists available at ScienceDirect

Journal of Power Sources

journal homepage: www.elsevier.com/locate/jpowsour

Short communication

Paradox phenomena of proton exchange membrane fuel cells operating under dead-end anode mode

Dong Jiang [a], Rong Zeng [a,*], Shumao Wang [a], Lijun Jiang [a], John R. Varcoe [b]

[a] Department of Energy Material and Technology, General Research Institute for Non-ferrous Metals, Beijing 100088, PR China
[b] Department of Chemistry, University of Surrey, Guilford GU2 7XH, UK

HIGHLIGHTS

- R_{hf}, *Va*, *Vc* concomitantly shift during the cell voltage drop of PEMFC in DEA mode.
- H_2 depletion tests reveal H_2O may accumulate at the catalyst/ionomer interface.
- Ultrathin PFSA film is key to understand the water transport in the catalyst layer.

ARTICLE INFO

Article history:
Received 6 December 2013
Received in revised form
17 April 2014
Accepted 17 April 2014
Available online 2 May 2014

Keywords:
Proton exchange membrane fuel cell
Water effect
Single electrode
Dead-end anode
H_2 depletion tests

ABSTRACT

By using two spatially separated reference electrodes in a single cell proton-exchange membrane fuel cell (PEMFC), the individual potentials of the anode and cathode are recorded under realistic operating conditions. The PEMFC is operated under dead-end anode (DEA) mode, without any humidification, to mitigate water accumulation at the anode. Although N_2 crossover from cathode to anode may play an important role in PEMFCs operating under DEA mode, our results unexpectedly show that the over-potentials of both the anode and cathode concomitantly increased or decreased at the same time. The increases of over-potentials correlate to the increase of the high frequency resistance of the cell (R_{hf}) imply that the water content in the membrane electrode assemblies is critical. However, the subsequent H_2 depletion tests suggest that water may accumulate at the interface between the surface of the catalyst and the ultrathin perfluorosulfonic acid (PFSA) ionomer film and this contradicts the above (the increase in R_{hf} implies the drying out of the MEAs). This study highlights the need for further research into understanding the water transport properties of the ultrathin PFSA ionomer film (<60 nm): it is clear that these exhibit completely different properties to that of bulk proton-exchange membranes (PEM).

1. Introduction

Proton-exchange membrane fuel cells (PEMFCs) represent a promising clean energy generation technology that is at the beginning of commercial application. The cost of the PEMFCs has been reduced by >80% since 2002. The cost of the Fuel Cell system for the vehicle has been reduced to \$49 kW^{-1} (in 2011) [1]. Although it is still \$19 kW^{-1} higher than the DOE 2015/2017 target, fuel cell vehicles are being introduced into the market (starting in Japan). However, the cost still needs to be reduced further for wide acceptance of fuel cell cars to be realized.

Fuel cells operating under dead-end anode (DEA) mode is of increasing interest [2–13] as control systems can be significantly simplified. However, water accumulation and the N_2 crossover (cathode → anode) are issues of concern [2–10]. However, the primary factors that are causing the significant drops in cell performance remain the subject of debate. By using neutron image technology, Siegel et al. [3] observed that accumulation of liquid water in the anode channels was followed by a significant drop in voltage when the air supply was fully humidified. Others argue that N_2 crossover from the cathode to the anode, when the fuel cell is operated under DEA mode, leads to a high concentration of N_2 and subsequent fuel depletion in the anode [6–8]: this will also cause the performance drop of the cell. In support of the latter, the performance of a DEA-mode fuel cell yielded a constant cell performance for 3 × longer periods of time when supplied with pure H_2 and O_2 compared to when H_2 and air supplies were used [8]. Meyer

* Corresponding author. Tel.: +86 10 82241241; fax: +86 10 82241294.
E-mail address: zengrong118@yahoo.com (R. Zeng).

http://dx.doi.org/10.1016/j.jpowsour.2014.04.086
0378-7753/

et al. [13] claimed that 50 ppm N_2 in the grade of H_2 used (BOC zero grade H_2 – likely to be widely used in such research work) leads to accumulation of N_2 at levels up to 2.3% in the anode of DEA PEMFCs (*i.e.* contributes to most of the N_2 observed in the anode). They also observed that the N_2 contents at the anode increased from 0.25% to 3% when the fuel cell was switched from flow mode to DEA mode. This highlights that the impurities in the H_2 supply need to be considered when discussing the effect of N_2 crossover from the cathode to the anode. However, the results presented in this study imply that the water content of the membrane electrode assemblies (MEA) is the critical factor that is responsible for the significant performance drops in cell performance. It is hypothesized that water accumulation at the interface between the catalyst surface and the ionomer plays an important role and that this needs to be subject to more detailed research.

2. Experimental details

A single cell with an active area of 19 cm^2 was employed in this study. Carbon paper electrodes, each containing a catalyst layer (Pt loading = 0.95 mg_{Pt} cm^{-2}) coated onto a micro-porous carbon layer, were hot-pressed onto 50 μm Nafion-212 proton-exchange membrane (PEM) to form the membrane electrode assemblies (MEAs). Nafion dispersion (5 wt% in isopropanol) was used as the binder to form the ionomer film in the catalyst layers. Pd coated Pt wires containing absorbed H [denoted as (Pt)PdH] [14] were used as *in situ* reference electrode (RE). Two spatially separated REs (one located at the anode side and the other at the cathode side) were used to independently record the potentials of anode and cathode under real-time fuel cell operation conditions. The details of the placement of the REs were as previously reported [15].

The fuel cell was operated in DEA mode with no external humidification at anode, *i.e.* the anode was supplied with dry H_2 (99.999%) via a pressure regulator. The H_2 purge was manually controlled by a valve at the outlet of the anode. A fuel cell test station with 8 auxiliary voltage detectors (Arbin FCTS 200W, USA) was used to control the other tests conditions: air flow rate = 6 × stoichiometry (unless otherwise specified) and air supply relative humidity (RH) = 0%, 25%, 50% and 80% (when testing the fuel cell with different cathode supply humidities). The impedance of the single cell was recorded using a PGSTAT302N potentiostat (Autolab, Switzerland) containing an electrochemical impedance spectrometer FRA2 module along with a 20 A booster. Two of the auxiliary voltage detectors of the Arbin FCTS were used to detect the potentials of the anode and cathode respectively. The potentials of the anode, cathode and the whole cell, along with the internal ohmic resistance of the cell (*i.e.* R_{hf}, the high frequency resistance), were recorded using the combination of the FCTS 200W and the PGSTAT302N to measure the performances of the fuel cells being operated in DEA mode. The small time differences between the operations of the two instruments were corrected using the cell voltages recorded by the two instruments (not shown in Figs. 1–3 for clarity but explained in detail in the caption of Fig. 4).

Micro-pinholes in the PEMs can cause significant N_2 crossover from cathode to anode. Considering the longevity of MEAs running under dry conditions and micro-pinholes in the membrane were previously observed when MEAs failed [9], each test was done using fresh MEA. The OCVs (open circuit voltages) of the MEA maintained the beginning-of-life values of 0.95–1.0 V after testing was completed: this simple test indicates the lack of micro-pinhole formation in the PEM. Unlike the failed MEAs in the longevity tests conducted by Yu et al. [8] and Matsuura et al. [9], scanning electron microscope (SEM) images of an unused MEA and a post test MEA show no detectable structural differences (Supplemental information: Fig. S1 shows the different zones of the MEA (in Fuel Cell test assemblies) that were studied and Fig. S2 presents the local SEM images of both the unused and used MEAs at different zones). This confirms the lack of significant micro-pinhole formation in the PEM.

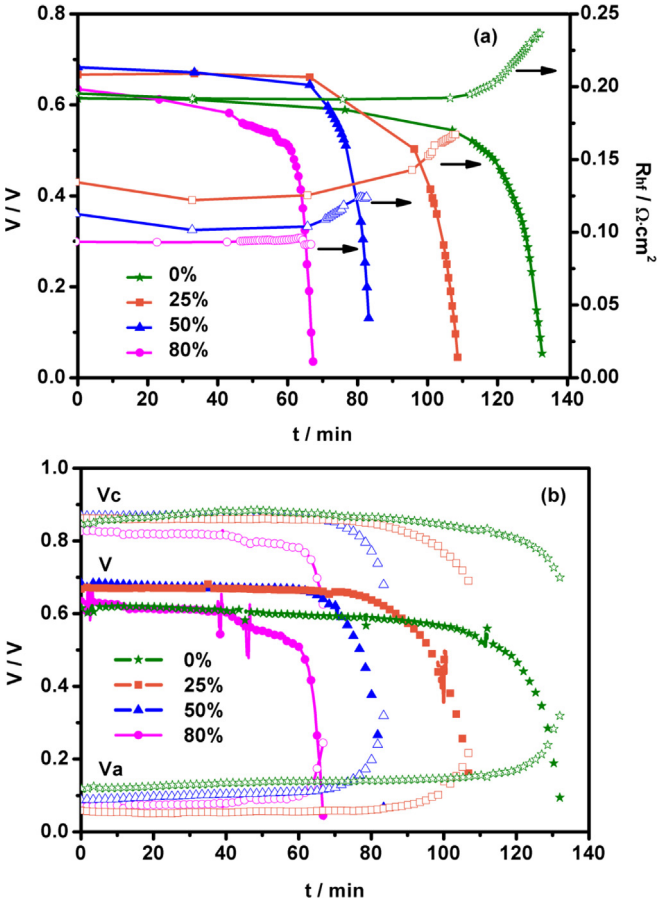

Fig. 1. (a) Chronopotentiometric and internal ohmic resistances (R_{hf}) of the DEA-mode fuel cells at 400 mA cm^{-2} with different air supply RHs. (b) The simultaneously recorded potentials of the anode (*Va*), cathode (*Vc*), and whole cell (*V*). T_{cell} = 50 °C, H_2 backpressure = 0.3 atm, anode RH = 0%, air supply = ambient pressure and 6 × stoich.

A test protocol was developed to aid the production of repeatable results: After the temperature of the cell and the RH of the air supply reached the set point, the cell was discharge at 0.2 V for *ca.*

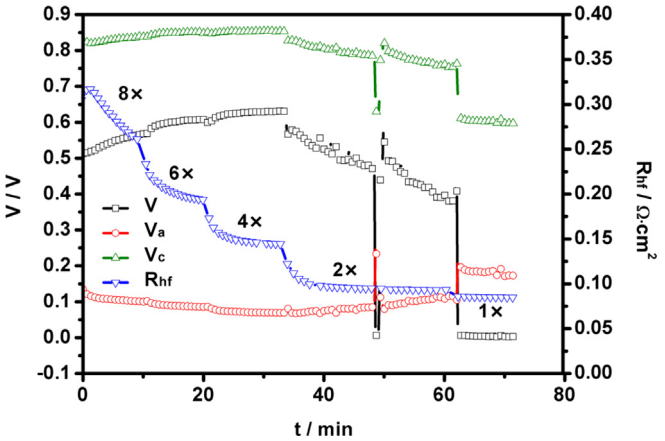

Fig. 2. The changes in the potentials of the anode, cathode, and whole cell and the R_{hf} values with discharge time for a DEA-mode fuel cell discharged at 400 mA cm^{-2} when supplied with air at different flow rates. T_{cell} = 50 °C, H_2 backpressure = 0.3 atm, anode and cathode RH = 0%, air supply = ambient pressure.

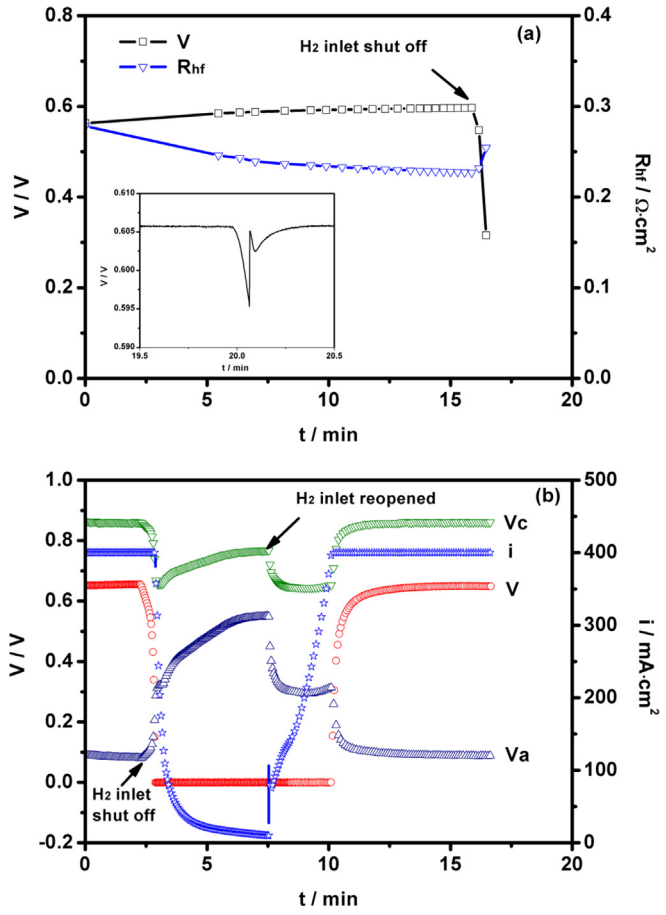

Fig. 3. (a) Chrono potentiometry curve and changes in R_{hf} at 400 mA cm^{-2} for a DEA-mode fuel cell (the inset graph shows the cell voltage response when the H_2 inlet was shut off for 5 s then reopened). (b) The potentials of the anode, cathode and the whole cell, along with the current response (initial discharge = 400 mA cm^{-2}), when the H_2 inlet was shut off and reopened deliberately (as indicated in the plot) during fuel cell operation. T_{cell} = 50 °C, H_2 backpressure = 0.3 atm, anode and cathode RH = 0%, air supply = ambient pressure and 6 × stoich.

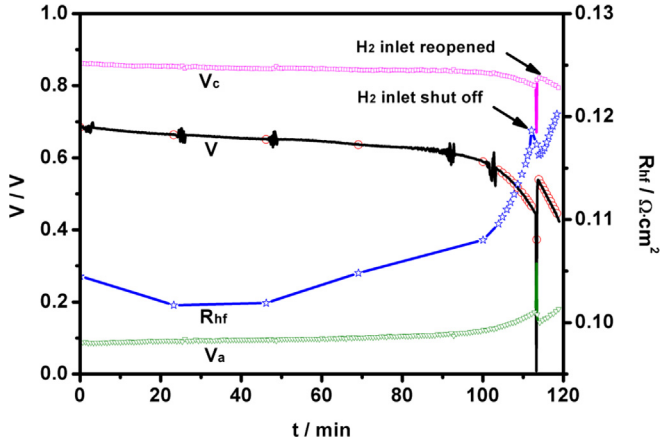

Fig. 4. The potentials of the anode, cathode, and the whole cell along with the R_{hf} values recorded with a DEA-mode fuel cell discharging with time at 400 mA cm^{-2}. The H_2 inlet was shut off and reopened deliberately as indicated in the plot. T_{cell} = 50 °C, H_2 backpressure = 0.3 atm, anode RH = 0%, air supply = ambient pressure, 6 × stoich and RH = 50%.

30 min in order to mitigate against transient effects between different tests under different conditions. The H_2 was purged during this 0.2 V discharge step. The cell was then maintained at OCV for 3 min. This procedure was used to ensure the MEA was fully balanced before formal testing was initiated. Typically, the fuel cell tests were repeated 3 times and data was discarded if the deviation of the potential of the RE was >40 mV unless otherwise specified. For clarity, the error bars are not shown in the plots presented in this paper: however, a typical repeatability test result can be found in Fig. S3 of the Supplemental information.

3. Results and discussion

The dramatic performance drop of fuel cells running in DEA mode has been ascribed to either water accumulation (at the anode) or N_2 crossover (from cathode → anode). This study is aimed at further elucidating the origins of this fuel cell performance drop.

Typical performances (at constant current) are presented in Fig. 1 (with a fuel cell discharge current of 400 mA cm^{-2}_{geo}). Fig. 1(a) shows that the R_{hf} generally decreases when the RH of the air supply is increased, which implies increased membrane and the ionomer hydration (and possible enhancement of water back diffusion from the cathode to anode). Cell voltage drops were observed in the later stages of the tests and commenced at the same time as the observed increases in R_{hf} (for each air supply RH apart from the RH = 80% condition where the performance of the cell dropped significantly with no observed increase in R_{hf}). This demonstrates a direct relationship between the cell R_{hf} and the sharp drops in cell performance and suggests that the performance drops (for the DEA-mode fuel cells) is unlikely to be caused by N_2 crossover as this would not affect the R_{hf} (*i.e.* the water content in the PEM or PFSA ionomer layers) in this way.

When the air was humidified to RH = 80%, the R_{hf} of the cell did not vary even when the performance of the cell decreased with time. Hwang et al. [16] suggested a pore-water morphology for Nafion PEMs with three water transitions in the membrane: (1) an adsorbed-layer percolation channel (adsorbed cluster → adsorbed layer water) transition that relates to the onset of the proton conductivity, (2) an adsorbed layer → capillary water transition that relates to the jump (increase) in proton conductivity at $\lambda_{H_2O} = 5$, (3) and a capillary water → flooding transition at $\lambda_{H_2O} > 7$. When λ_{H_2O} were in the range 5–7, the proton conductivities were in range 0.02–0.04 S cm^{-1} at 80 °C. The *in situ* conductivities (calculated from R_{hf}) of cells at 50 °C with cathode RHs = 80%, 50%, 25%, and 0% RH were 0.054, 0.048, 0.040, and 0.026 S cm^{-1} respectively. Considering this data, it is plausible that the pore water of the Nafion was *ca.* $\lambda_{H_2O} = 5$–7 for the fuel cells operating with RH = 0–50%. The immediate increase in R_{hf}, when the voltage of the cell drops, may reflect the capillary water → adsorbed-layer water transition. In case of RH = 80%, no such water transition may exist and, hence, R_{hf} did not measurably increase. The operation of DEA-mode fuel cells under relatively dry conditions (H_2 RH = 0% and air RH = 0–50% RH) mitigates against water accumulation in the GDLs and MPLs but still reflects the changes in water contents in the catalyst layers.

The over-potential of anode increased as expected as seen in Fig. 1(b). However, the over-potential of cathode also increased (at the same time). When operated in the reported DEA mode, the concentration of N_2 at the fuel cell cathode should remain constant (with high stoichiometric air supplies) and the over-potential of cathode would be expected to remain constant (assuming unchanged water/hydration effects as the cell is operated under the same condition during the whole test) even if the cell voltages decreased due to N_2 crossover (cathode → anode). Our data shows

that this is not the case. The reactions at the anode and cathode are different so the simultaneous increases in over-potential (at the anode and cathode) suggest a common factor is responsible for the observed cell performance losses.

When considering the concomitant increase in R_{hf} with the increased over-potentials at both electrodes, the losses in cell voltage must relate to the water content in the PEM or PFSA ionomer in the catalyst layers. If the cell voltage losses were caused by the dehydration of the MEA, one would expect the cell voltage losses to occur earlier with the decreased RHs at the cathode. However, this is not the case. Lee et al. [5] also reports this kind of phenomenon. Hence, we believe the cell voltage losses are not caused by the dehydration of the MEA.

Additional O_2 depletion and H_2 depletion tests were conducted deliberately before cell performance drops were observed in order to rule out any effect from N_2 and water accumulation at the anode. The outlet of the anode was closed during the fuel cell operation. By decreasing the air flow rate from 8 × stoich to 1 × stoich, the fuel cell would be increasingly operated under a condition of O_2 depletion (Fig. 2). The cell resistance decreased as expected due to the increased back diffusion of water from cathode to anode with the slower cathode flow rates (along with the simultaneous shift of the potential of anode, cathode, and the whole cell). The fuel cell was operated under H_2 depletion conditions by closing the H_2 inlet as shown in Fig. 3. The R_{hf} (Fig. 3(a)) increased as expected on shutting the valve (cutting off the H_2 supply). The inset graph in Fig. 3(a) shows the cell voltage changed (when the fuel cell was discharging normally at 400 mA cm^{-2}) after shut off of the H_2 inlet (for 5 s) and after reopening. A sudden drop in cell voltage (from 606 mV to 595 mV) was observed on closure of the H_2 inlet. The cell voltage then recovered back to 605 mV on opening of the inlet, decreased again to 602 mV, and finally increased slowly back to the initial value of 606 mV. The pulse in voltage was caused by the changes in H_2 flow rate and the increase in cell resistance during inlet shut off and reopening step. To explore the potential shifts at the anode and cathode, the H_2 inlet was closed for 5 min and then reopened again [data shown in Fig. 3(b)]. After a period of time after the inlet of H_2 was reopened, the cell performance recovered. The over-potentials of anode and cathode and the R_{hf} shifted simultaneously during both (H_2 and O_2) depletion tests (consistent with the tests in Fig. 1). As R_{hf} values reflect the water content in the MEA, the observation of simultaneous changes of the potential of the cell, the over-potentials of anode and cathode, and the R_{hf} confirms that water effects are likely responsible for the loss of cell performance with time.

To further understand the observations in the initial H_2 depletion test above, the H_2 inlet was shut off for 5 s (shut off initiated when a cell voltage of 0.45 V was reached) and then reopened again (the outlet remained closed for the entire process, see Fig. 4). The cell voltage (circles in Fig. 4) and the R_{hf} (stars in Fig. 4) data were recorded by the Autolab instrument. The potential of anode, cathode and the whole cell were recorded at the same time using the Arbin instrument (with an inter-instrument time base correction via the cell voltages recorded by the Arbin instrument [lines in Fig. 4] and the Autolab [circles in Fig. 4]). The fuel cell was discharged at constant current density (400 mA cm^{-2}) in DEA mode. This test ensures that accumulation of N_2 and H_2O can occur (*i.e.* they are not purged from the anode). The inlet shut off process caused the voltage performance of the cell to drop further. It was expected that the voltage of the cell would not recover over 0.45 V when the H_2 inlet was reopened. However, the voltage of the cell recovered to 0.52 V immediately the H_2 inlet was reopened: this shows a completely different behavior from the test that generated the data in the inset of Fig. 3(a). This confirms that the increased in cell voltage (70 mV more than the value before H_2 inlet closure) was not caused by the fluctuation of H_2 flow rate due to the shut off and reopened inlet.

The R_{hf} increased on shut off of the H_2 inlet. As the cell was discharging at 400 mA cm^{-2} when the inlet of H_2 was closed, the H_2 would be quickly depleted and the pressure at anode would be decreased. The increased R_{hf} indicates the evaporation of water (including any that has accumulated in the MEA) due to this reduced pressure at the anode. It is also understandable that the R_{hf} value decreased again when the H_2 inlet was reopened, as the pressure of H_2 in the anode recovered leading to the balance of water (between the gas and the MEA) recovering back to the initial state (to that prior to the closure of H_2 inlet). However, the increased 70 mV in cell voltage could not be caused by the decreased in R_{hf} after inlet reopening (this is calculated to contribute $<$ 1 mV). This data therefore supports the hypothesis that the H_2O was desorbed at the surface of the catalyst. The over-potentials of the anode and cathode both decreased (when the cell voltage increased to 0.52 V), which implies that there are an increased number of active sites for both the ORR and HOR reactions. This is consistent with the adsorption energies of N_2 and H_2O on Pt surface being $<$1 eV [17,18] (adsorption energy of N_2 = 0.158 eV for an unconstrained N_2 monolayer [18] and the absorption energy of H_2O is up to 0.5 eV depending on the structure of Pt surface and the state of adsorbed H_2O {*e.g.* monomer, dimer, or trimer} [17]). The higher adsorption energy for H_2O implies that adsorbed H_2O will play a more important role compared to absorbed N_2, which is in agreement with the experimental results (*i.e.* the R_{hf} increased [H_2O desorption] when the H_2 inlet was shut).

It is a paradox that the R_{hf} increases when water is accumulating at the interface between the surface of catalyst and the ionomer films. However, this situation can exist due to the different characteristics of the thin ionomer film (covering the surface of the catalyst in the CLs) compared to the bulk PFSA membrane (*i.e.* Nafion PEM). TEM images of the PFSA ionomer coated catalyst in the CLs of our MEA confirmed the thickness of the PFSA ionomer film to be in the range 2–10 nm (as shown in Fig. 5). By using sum frequency generation spectroscopy (SFG), Noguchi and coworkers [19] show that the interface between the PFSA thin film and the Pt surface is different from the interface between PFSA and a HOPG

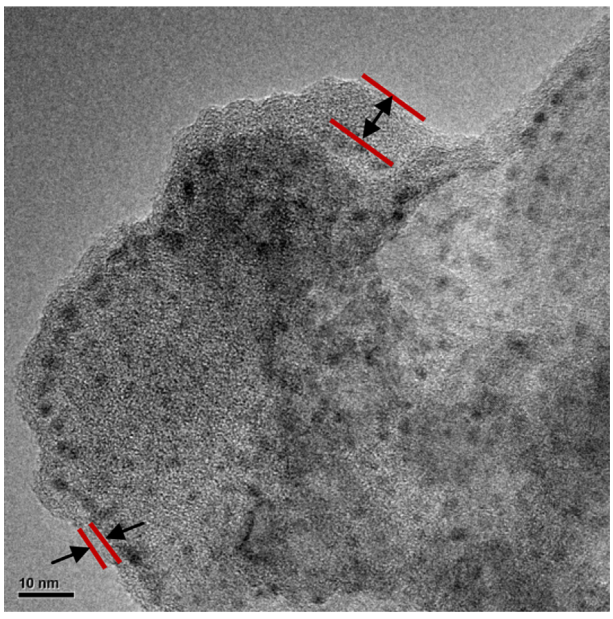

Fig. 5. The TEM graph for the catalyst covered with the PFSA ionomer film.

surface. A peak *ca.* 3600 cm^{-1}, that corresponds to water molecules interacting with the sulfuric acid groups in proton channel at PFSA surface, was observed in the SFG spectra (in the OH stretching region) for both of the Pt/PFSA and HOPG/PFSA interfaces. However, while the intensity of this IR band increased with RH for the PFSA/Pt interface, no increase was observed for the PFSA/HOPG interface. This suggests that water is more prone to accumulate at the PFSA/Pt interface rather than the PFSA/carbon interface. The work of Page et al. [20,21] shows that the humidity dependent equilibrium swelling ratio, volumetric water fraction, and effective water diffusivity was much lower in a PFSA ultrathin film (<60 nm) on a silicon wafer compared to a thicker film (60–250 nm). The water transport kinetics in a thin film on a hydrophilic or a hydrophobic substrate is the same [21]. Page et al. suggest that the retardation in the transport kinetics in ultrathin films, compare to thicker films, is not due to the interfacial morphology of the transport domains but rather a general effect of confinement [21]. Paul et al. [22] found that ultrathin films (<55 nm) exhibited hydrophilic surface characteristics, whereas thicker films (>55 nm) exhibited hydrophobic surface characteristics (as seen with bulk Nafion PEM). All of these cited prior works suggest that PFSA ionomer ultrathin films (<*ca.* 60 nm) have different properties compared to those of bulk Nafion. However, it is still not clear how the ultrathin ionomer films affect the water distribution at the interface between the catalyst and the ionomer under real operating conditions. Although caution is warranted when transferring the limited pool of knowledge regarding ultrathin PFSA films to a real world catalyst/ionomer interface (due to the different interface properties regarding ultrathin films and substrates in the literature), our results are still consistent with the hypothesis that water accumulates at the interface even when the membrane or the ionomer film is dry (due to the lower water diffusivities of ultrathin ionomer films compared to bulk PEMs). The ultrathin ionomer films are less capable of adsorbing water and water can, therefore, more easily accumulate at the catalyst/ionomer interface (as stated, even if the fuel cell is operated under relatively dry conditions). This water accumulation at the catalyst/ionomer interface can cause the H_2 depletion at the anode and result in a performance drop (drop in cell voltage). The reason why R_{hf} simultaneously increases with increases in anode and cathode overpotentials (*i.e.* with the significant drop in cell voltage), the effect of the ultrathin PFSA ionomer films on the performance of the cell, and the resulting H_2 depletion effects on the performance of the cell are all subjects that need to be studied in detail in the future.

Although the significant performance drop of H_2/air fuel cell is unlikely to be due to the effect of the N_2 crossover (cathode → anode), the fuel cell supplied with RH = 0% H_2 and O_2 showed no significant drop in cell performance drop over 500 min of testing, while a comparable fuel cell supplied with RH = 0% H_2 and air did show significant drop in cell performance over only 100 min (both experiments at 400 mA cm^{-2}); this observation was consistent with those of Yu et al. [8]. This indicates that the presence of N_2 is still important but further investigations are required to elucidate what exactly is going on.

4. Conclusion

The experimental results show that the over-potential of anode and cathode and the high frequency resistance (R_{hf}) values all concomitantly increased during temporal drops in cell voltage for proton-exchange membrane fuel cells operating in dead-end anode (DEA) mode. This implies a close relationship between the overpotential of anode and cathode and the cell resistance. The current work provides a hypothetical mechanism to explain these observations. The MEA needs to be considered as a whole and it is hypothesized that water accumulates at the interface between the surface of the catalyst and the ultrathin ionomer film resulting in H_2 depletion at the anode. Further studies on this phenomenon are needed and will lead to deeper insights into the fundamental electrochemical processes occurring in the catalyst layers. It also highlights the need for further studies into the properties of ultrathin (<60 nm) PFSA films and its effect on water diffusion and distribution in the catalyst layers of the MEAs under the real fuel cell operating conditions.

Acknowledgments

We are grateful to the Foundation of General Research Institute for Non-ferrous Metals (GRINM, Grant No. 52208) for financial support of this work. The valuable discussions with Dr. Ligen Wang at GRINM are also greatly appreciated. John Varcoe is holder of an EPSRC (UK) Leadership Fellowship (grant EP/I004882/1).

Appendix A. Supplementary data

Supplementary data related to this article can be found at http://dx.doi.org/10.1016/j.jpowsour.2014.04.086.

References

[1] DOE Hydrogen and Fuel Cells Program Record – Fuel Cell System Cost 2011 – Record #11012, 17.8.2011.
[2] Y. Lee, Y.H. Jang, T. Jung, J.T. Chung, Y. Kim, ECS Trans. 3 (2006) 871–878.
[3] J.B. Siegel, D.A. McKay, A.G. Stefanopoulou, D.S. Hussey, D.L. Jacobson, J. Electrochem. Soc. 155 (2008) B1168–B1178.
[4] A.P. Sasmito, A.S. Mujumdar, Int. J. Hydrogen Energy 36 (2011) 10917–10933.
[5] Y. Lee, B. Kim, Y. Kim, Int. J. Hydrogen Energy 34 (2009) 7768–7779.
[6] K.D. Baik, M.S. Kim, Int. J. Hydrogen Energy 36 (2011) 732–739.
[7] J.B. Siegel, S.V. Bohac, A.G. Stefanopoulou, S. Yesilyurt, J. Electrochem. Soc. 157 (2010) B1081–B1093.
[8] J.L. Yu, Z.W. Jiang, M. Hou, D. Liang, Y. Xiao, M.L. Dou, Z.G. Shao, B.L. Yi, J. Power Sources 246 (2014) 90–94.
[9] T. Matsuura, J.X. Chen, J.B. Siegel, A.G. Stefanopoulou, Int. J. Hydrogen Energy 38 (2013) 11346–11356.
[10] A. Rabbani, M. Rokni, Appl. Energy 111 (2013) 1061–1070.
[11] J.X. Chen, J.B. Siegel, T. Matsuura, A.G. Stefanopoulou, J. Electrochem. Soc. 158 (2011) B1164–B1174.
[12] J.X. Chen, J.B. Siegel, A.G. Stefanopoulou, J.R. Waldecker, Int. J. Hydrogen Energy 38 (2013) 5092–5105.
[13] Q. Meyer, S. Ashton, O. Curnick, T. Reisch, P. Adcock, K. Ronaszegi, J.B. Robinson, D.J.L. Brett, J. Power Sources 254 (2014) 1–9.
[14] R. Zeng, S.D. Poynton, J.P. Kizewski, R.C.T. Slade, J.R. Varcoe, Electrochem. Commun. 12 (2010) 823–825.
[15] R. Zeng, R.C.T. Slade, J.R. Varcoe, Electrochim. Acta 56 (2010) 607–619.
[16] G.S. Hwang, M. Kaviany, J.H. Nam, M.H. Kim, S.Y. Son, J. Electrochem. Soc. 156 (2009) B1192–B1200.
[17] L. Árnadóttir, E.M. Stuve, H. Jónsson, Surf. Sci. 604 (2010) 1978–1986.
[18] P. Zeppenfeld, R. David, C. Ramseyer, P.N.M. Hoang, C. Girardet, Surf. Sci. 444 (2000) 163–179.
[19] H. Noguchi, K. Taneda, H. Naohara, K. Uosaki, Electrochem. Commun. 27 (2013) 5–8.
[20] S.A. Eastman, S. Kim, K.A. Page, B.W. Rowe, S. Kang, C.L. Soles, Macromolecules 45 (2012) 7920–7930.
[21] S. Kim, J.A. Dura, K.A. Page, B.W. Rowe, K.G. Yager, H.J. Lee, C.L. Soles, Macromolecules 46 (2013) 5630–5637.
[22] D.K. Paul, K. Karan, A. Docoslis, J.B. Giorgi, J. Pearce, Macromolecules 46 (2013) 3461–3475.